Adaptive Decomposition and Multitimescale Analysis of Long Time Series of Climatic Factors and Vegetation Index Based on ICEEMDAN-SVM

Qianqian Sun, Chao Liu, Tianyang Chen, Anbing Zhang, Chunyang Liu, and Yuan Tao

***Abstract*—Climate change is of great significance to vegetation coverage. However, the long time series of climatic factors and vegetation index are nonstationary and nonlinear, containing different information in frequency and time scales. The study innovatively integrated a support vector machine (SVM) and improved complete ensemble empirical mode decomposition with adaptive noise (ICEEMDAN), and analyzed the relationship between climatic factors and the normalized difference vegetation index (NDVI) at three timescales in Loess Plateau (LP). The results indicate that: 1) The mode mixing phenomenon of empirical mode decomposition can be better solved by using ICEEMDAN, and the end effect can be mitigated by using SVM to expand both ends of the data before decomposition. 2) The residual NDVI stripped out using ICEEMDAN-SVM can represent the long-term trend of the original data. The results show that the NDVI and climate factors performed noticeable spatial and temporal differences under different climate zones. 3) The relationship between vegetation and climatic factors revealed obvious spatial heterogeneity at different timescales, and the climate change in the overall trend explained the vegetation change to the greatest extent, approximately 95%. The study has shown that temperature is a limiting factor affecting the growth of vegetation on the LP. We propose ICEEMDAN-SVM to study the relationship between climate factors and vegetation indices at multiple timescales, revealing some hidden information in long time series and providing a new method to quantify the impact of climate change on vegetation dynamics.**

***Index Terms*—Climate change, improved complete ensemble empirical mode decomposition with adaptive noise (ICEEMDAN), Loess Plateau (LP), multiple timescales, normalized difference vegetation index (NDVI), support vector machine(SVM).**

Manuscript received 6 June 2022; revised 13 July 2022; accepted 21 July 2022. Date of publication 29 July 2022; date of current version 10 August 2022. This work was supported in part by the National Natural Science Foundation of China under Grant 42071246, in part by the Natural Science Foundation of Hebei Province under Grant E2020402006, and in part by the Natural Science Foundation of Anhui Provincial under Grant 2108085MD130. *(Corresponding author: Chao Liu.)*

Qianqian Sun, Chao Liu, and Chunyang Liu are with the School of Spatial Informatics and Geomatics Engineering, Anhui University of Science and Technology, Huainan 232001, China (e-mail: qianqiansun@my.swjtu.edu.cn; chliu1@aust.edu.cn; chunyangliu@aust.edu.cn).

Tianyang Chen is with the Department of Geography and Earth Science, The University of North Carolina at Charlotte, Charlotte, NC 28223 USA (e-mail: tchen19@uncc.edu).

Anbing Zhang is with the School of Mining and Geomatics, Hebei University of Engineering, Handan 056038, China (e-mail: zhang-anbing@hebeu.edu.cn).

Yuan Tao is with the School of Environment Science and Spatial Informatics, China University of Mining and Technology, Xuzhou 221116, China (e-mail: yuantao@cumt.edu.cn).

Digital Object Identifier 10.1109/JSTARS.2022.3194987

I. Introduction

VEGETATION is an essential component in the terrestrial ecosystem, and it is affected by the interaction of the carbon, hydrological, and energy cycles in terrestrial and atmospheric systems [1]–[4]. The long-time series of vegetation index and climatic factors are nonstationary and nonlinear and include different frequency information [5]–[7] such as monthly, seasonal, annual, interannual, and short- or long-term changes [8]–[11]. Therefore, the problem is to separate the different timescales of the long time series.

Currently, some studies depend on normalized difference vegetation index (NDVI) data to investigate the connection between vegetation dynamics and climate change[12]–[15]. For instance, Bao et al. [16] explored the changing trend of vegetation and its response pattern to seasonal climatic factors from 2001 to 2010 in the Mongolian Plateau. Chen et al. [17] studied the annual vegetation change using NDVI from 1982 to 2011 in the Asia-Pacific region. Rishmawi et al. [18] explored the response mechanism of NDVI to different climate variables at the interannual scale from 1982 to 2006. Bunting et al. [19] recovered the lag effect of climate change on vegetation on a monthly scale in the southwestern United States. All the above studies are directly analyzed using the traditional time series analysis method under the assumption of linearity and stationarity.

Considering the datasets of NDVI and the climatic factors are nonlinear and nonstationary, we analyze the long time series of vegetation index and climate variables using the multiple timescale decomposition method. There are many decomposition tools to separate long time series into different timescales, such as spectral analysis [20]–[22], wavelet analysis [23]–[25], multiresolution analysis [11], [26], and time-series satellite data analysis tool [27]. These methods cannot identify the temporal and spatial patterns in long time series and there is no quantitative method that focuses on seasonal and interannual fluctuations [24], [28]. Although wavelet analysis can divide long time series into time–frequency space and has been widely used in geophysical research, it lacks quantitative results and self-adaptability in studies [29].

In addition, some scholars have tried to use the decomposition method, such as empirical mode decomposition (EMD), ensemble empirical mode decomposition (EEMD), and complete ensemble empirical mode decomposition with adaptive noise (CEEMDAN) to conduct multiple timescale

analyses on long-term geospatial data (e.g., remote sensing images, climate data, and hydrological elements) [30]–[33]. Verma and Dutta [34] used EMD to analyze the NDVI time series to obtain different traits of vegetation phenology and confirmed the significance of vegetation change trend by nonparametric seasonal mann–kendall test. Chen et al. [35] integrated EMD and redundancy analysis to show temporal and spatial differences in the enhanced vegetation index, precipitation, and temperature and analyzed the partial effect of precipitation and temperature on primary productivity. Qi et al. [36] used EEMD and residual trend methods to explore the relationship between climate change, human activities, and vegetation index on multiple timescales in China's Silk Road Economic Belt. They indicated that the time series of vegetation could be divided into 3- and 6-year timescales and long-term trends. Moreover, climatic factors mainly affected vegetation changes over short timescales. Zhang et al. [37] analyzed the vegetation cover changes at different temporal and spatial scales, and their correlation with climate change depended on EEMD. Liu et al. [38] used CEEMDAN and fast Fourier transformation (FFT) methods to explore the temporal and spatial variations of vegetation and its relationship with temperature and precipitation in the Inner Mongolia Plateau, China. The outcomes indicated that the long time series of vegetation and temperature had 1-year and half-year cycles, whereas the period of precipitation was a 1-year cycle.

EMD is developed initially from the engineering domain, aiming to decompose a signal into named intrinsic mode functions (IMF) along with a trend [39], which has two problems, i.e., mode mixing and end effect [40]–[42]. Improved complete ensemble empirical mode decomposition with adaptive noise (ICEEMDAN) is the cutting-edge member belonging to the EMD family to gain components with stronger physical meaning and less noise from a long-term sequence, which can alleviate the problem of mode mixing [43]. The end effect is a problem throughout the whole family of EMD [41], [42], where both ends of the long-term sequence to be decomposed will cause data distortion because they are not continuous like those points in the middle. The effect may also lead to a biased conclusion on addressing research questions in the geographic domain. So, the study uses the algorithm of machine learning to add a certain number on both sides of the original data, which can effectively suppress the end effect problem. support vector machine (SVM) is a method in machine learning. At present, some scholars have proved the SVM can be an excellent way to mitigate the problem of end effect in the EMD family [44]–[48].

Based on the two problems proposed above, we innovatively integrate ICEEMDAN and SVM into ICEEMDAN-SVM, to study the long time series of NDVI and climatic factors (temperature and precipitation) of Loess Plateau (LP) from 1982 to 2015 to obtain components at different timescales, and then use FFT to conduct the spectrum analysis of different components [22], [49], [50]. The main objectives of this article are as follows:

1) using ICEEMDAN and SVM methods to reduce the effects of the mode mixing and end effect problems;
2) analyzing the change trends of vegetation NDVI, temperature, and precipitation and detecting the performance of the long-term trend of NDVI;
3) analyzing the relationship between vegetation types and their corresponding climatic factors in different timescales.

II. Materials and Methods

A. Study Area

The LP is located between longitudes 100° 54′ E to 114° 33′ E and latitudes 33° 43′ N to 41° 16′ N, which belongs to the upper and middle reaches of the Yellow River of China [51]. Its area is approximately 640 000 km^2 and the altitude is 800–3000 m. It has a complex landform, productive geological environment, severe soil erosion, and a frail ecological system [52], [53]. The annual precipitation is 150–750 mm and the annual mean temperature is 3.6–14.3°C. The vegetation types in the LP are mainly evergreen broad-leaved mixed forests, desert steppe, typical steppe, and forest-steppe [54], [55]. Fig. 1 exhibits the spatial distribution of different vegetation types and three climate zones of the LP.

B. Datasets

The NDVI product has 15-day intervals with 0.083° spatial resolution, belonging to the third generation Global Inventory Monitoring and Modeling System (GIMMS NDVI3g) dataset [56]. The dataset was carefully calibrated to minimize the harmful impacts including volcanic eruptions and orbital drift [56], [57]. Its long time series variation indicates the true character of vegetation activity changes [58]–[61]. The NDVI data were obtained according to the maximum value composite method to decrease the effect of clouds and aerosols on the atmosphere [62]

$$\mathrm{NDVI}_i = \mathrm{Max}\left(\mathrm{NDVI}_{i1}, \mathrm{NDVI}_{i2}\right) \tag{1}$$

where NDVI_i is the NDVI for the ith month, NDVI_{i1} is the NDVI for the first 15 days of the ith month, and NDVI_{i2} is the NDVI for the last 15 days of the ith month. To avoid the impact of winter and early spring extreme weather on the vegetation, the growing season for this study was chosen from April to October [63], [64] and used the datasets from the growing season to conduct research.

The climate datasets were obtained from the Chinese Climate Academic and Science Dataset (http://cdc.cma.gov.cn/), which includes, but is not limited to, monthly mean temperature and accumulative precipitation from 52 meteorological stations of LP. To obtain the identical temporal and spatial resolution as NDVI data, we used the inverse distance weighting method for climate datasets from 1982 to 2015 [65].

Land cover data are retrieved from MODIS products (MCD12C1) with 0.05° spatial resolution and 17 land-cover types (see Table I). We adopted the identified land cover dataset from 2001 to 2012 and further selected those pixels that had not been changed in this period. Moreover, we omitted those make-believe land (e.g., farmland) since their greenness could be more impacted by human activities rather than climate change. Finally, three vegetation types, i.e., mixed forests, grasslands, and barren or sparsely vegetated, are applied to analyze the relationship

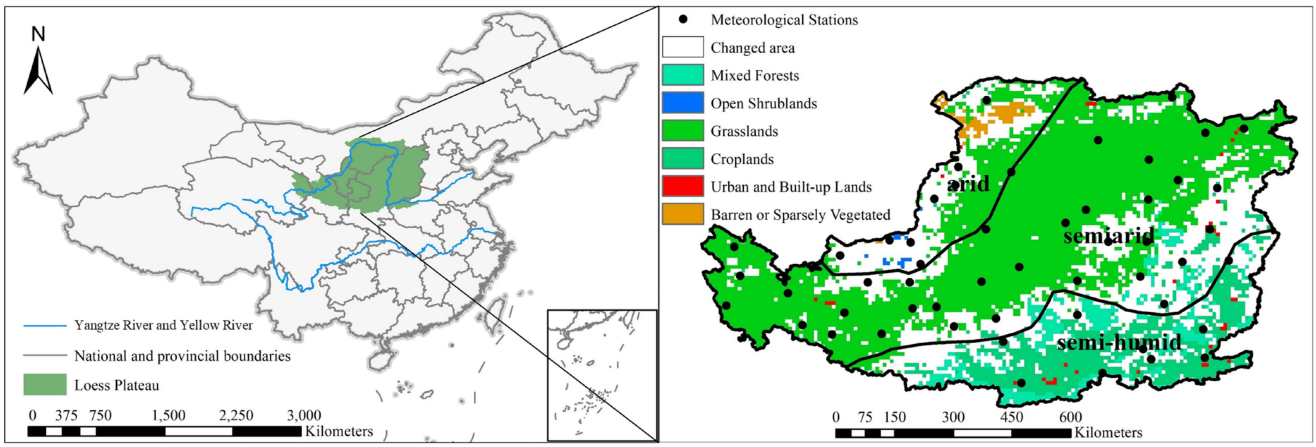

Fig. 1. Spatial distribution of different vegetation types and three climate zones of the LP.

TABLE I
INTERNATIONAL GEOSPHERE–BIOSPHERE PROGRAM LAND COVER CLASSIFICATION

Value	Description	Value	Description
0	Water Bodies	9	Savannas
1	Evergreen Needleleaf Forests	10	Grasslands
2	Evergreen Broadleaf Forests	11	Permanent Wetlands
3	Deciduous Needleleaf Forests	12	Croplands
4	Deciduous Broadleaf Forests	13	Urban and Built-Up
5	Mixed forests	14	Cropland/Natural Vegetation Mosaic
6	Closed Shrublands	15	Permanent Snow and Ice
7	Open Shrublands	16	Barren or sparsely vegetated
8	Woody Savannas	17	Unclassified

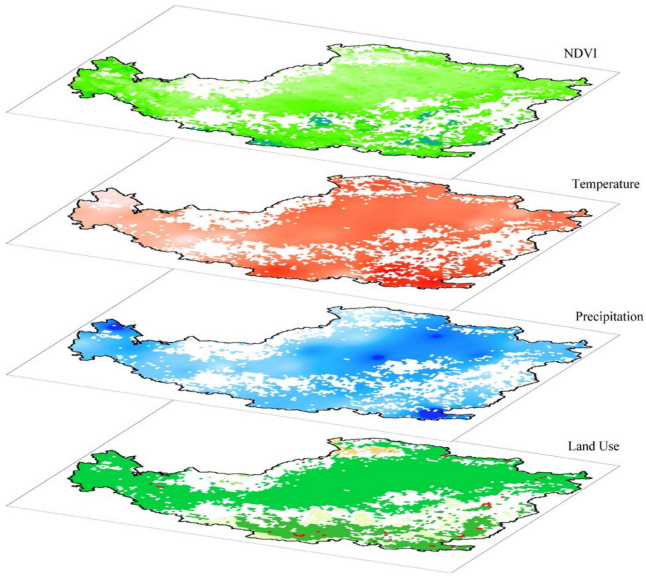

Fig. 2. GIS data layers of LP.

between vegetation and climate change. The interpolated surface of climatic factors and land cover data were resampled to obtain the identical format as the NDVI product so that each greenness value corresponds to the values of a set of climatic factors and land cover data (see Fig. 2).

The relationship between vegetation and climate is very complicated and closely dependent on regional effects, such as regional soil, landform, and vegetation types [66], [67]. According to the climatic regions in Fig. 1, the vegetation types have been divided into six categories in Table II.

C. Analysis Methods

Two problems are embedded in the EMD family, i.e., mode mixing and end effect [40]–[42]. The development of EMD has been centering on mitigating the impact of these problems. ICEEMDAN, the cutting-edge method in the EMD family in this study, mitigates the impact of mode mixing. Moreover, the SVM can suppress the end effect [44], [68] problem by adding a certain number of points on both sides of the original data. The principles of the ICEEMDAN and SVM are demonstrated in the following sections.

TABLE II
DIVIDING ORIGINAL DATA INTO SIX CATEGORIES BASED ON THREE CLIMATE ZONES AND THREE TYPES OF NATURAL VEGETATION

Vegetation Type	Label	Area Percentage (%)
Arid Grasslands	AG	5.43
Arid Barren or sparsely vegetated	AB	1.02
Semiarid Mixed forests	SAF	1.19
Semiarid Grasslands	SAG	44.31
Semihumid Mixed forests	SHF	3.90
Semihumid Grasslands	SHG	0.57

1) Improved Complete Ensemble Empirical Mode Decomposition With Adaptive Noise (ICEEMDAN): The ICEEMDAN is the latest member in the EMD family,

where EMD is a method derived from the Hilbert–Huang transform [39]. EMD is a time–frequency analysis method with local adaptive characteristics, which is mainly used to analyze nonstationary signals from nonlinear systems. The above-mentioned method can decompose a signal into multiple IMF components and a residual [38], [39], [47]. In geography, scholars treat IMF in specific frequencies as cycles in corresponding timescales (e.g., annual and interannual scales) [69]–[71]. The basic principle of the EMD is as follows. For the original data $f(t)$, we obtain the extreme point of $f(t)$ and generate the upper and lower envelopes via linking all local maxima and minima with cubic spline interpolation, respectively. Next, $f(t)$ minus the means of upper and lower envelopes. Repeating the above steps, until it satisfies the stopping criteria that it cannot extract IMFs. That can obtain a finite number of basic mode components $\mathrm{imf}_j(t)$ and the residual term $r_n(t)$. The expression is as follows:

$$f(t) = \sum_{j=1}^{n} \mathrm{imf}_j(t) + r_n(t). \tag{2}$$

The ICEEMDAN is proposed by Colominas et al. [43], which adds a certain amount of Gaussian white noise to original data so that the data has continuity between different components. It generates new extreme points, which can reduce the mode mixing phenomenon. When it comes to a geographic domain, we can assume the long-term sequences of NDVI or climatic factor is x. Therefore, the algorithm can be described as follows.

1) Add a certain amount of Gaussian white noises to the long-term sequence x. The signal to be decomposed is as follows:

$$x^i = x + \beta_0 \cdot E_1\left(w^i\right) \tag{3}$$

where x^i is the signal to be decomposed with white noise, and i is the number of times to add white noise, where $i = 1, 2, \ldots, n$. β_0 is the size of the noise, w^i is the zero mean unit variance white noise, and $E_1(w^i)$ is the first EMD component of w^i.

2) IMF_1 of ICEEMDAN was obtained by decomposing x^i using EMD. That is

$$\mathrm{IMF}_1 = x - \left\langle M\left(x^i\right)\right\rangle \tag{4}$$

where $\langle\cdot\rangle$ is to achieve averaging and $M(\cdot)$ is the operator which produces the local mean of the signal.

3) Assess the second residual as the local average of the realization $\langle M(x^i)\rangle + \beta_1 \cdot E_2(w^i) = r_1 + \beta_1 \cdot E_2(w^i)$, and define the second component

$$\mathrm{IMF}_2 = r_1 - \left\langle M\left(r_1 + \beta_1 \cdot E_2\left(w^i\right)\right)\right\rangle. \tag{5}$$

4) In the same way, the kth signal to be decomposed is $r_{k-1} + \beta_{k-1} \cdot E_k(w^i)$. Compute the kth mode

$$\mathrm{IMF}_k = r_{k-1} - \left\langle M\left(r_{k-1} + \beta_{k-1} \cdot E_k\left(w^i\right)\right)\right\rangle. \tag{6}$$

5) Repeat step (4) when the obtained residual is a monotonic function that is unable to decompose again.

2) Support Vector Machine (SVM): The SVM method was put forward by Vapnik [72], which is one of the most commonly used tools in many fields, including geography [46]. SVM uses pattern recognition to find the optimal separation plane in the linearly separable problem to classify the data nonlinearly (see Fig. 3).

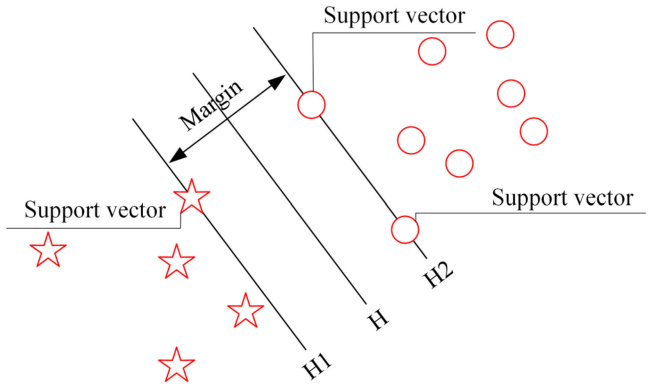

Fig. 3. Optimal separating line of SVM.

Using nonlinear mapping Φ to map data x to a high-dimensional feature space F and to perform linear regression in this feature space is the basic principle of SVM for regression. x includes NDVI, precipitation, and temperature.

$$f(x) = \omega \cdot \Phi(x) + b, \Phi \cdot R^n \to F, \omega = F \tag{7}$$

where ω represents the weight vector, b represents bias, and R^n represents an n-dimensional vector.

The main advantage of SVM is that it employs the structural risk minimization (SRM) principle, which has been shown to outperform the empirical risk minimization (ERM) principle used by traditional neural networks. SRM seeks to minimize an upper bound on the generalization error consisting of the sum of the training error and the confidence level based on the Vapnik–Chernoverkis dimension, which is different from the commonly used ERM principle that only minimizes the training error. This method has proven to be very effective for solving generic classification and regression problems [73]–[75]. The basic idea of SVM for regression is to introduce kernel function, map the input space into a high dimensional feature space via a nonlinear mapping, and perform a linear regression in this feature space [72].

3) Demonstrate the Result of the Simulation Signal by Integrating ICEEMDAN and SVM: The ICEEMDAN can reduce the impact of the issue of mode mixing, but the end effect is not resolved. The SVM mitigates the end effect, but there is still uncertainty at both ends of the signal after extending. Therefore, that needs to notice that the SVM extension can only mitigate the impact of the end effect and does not eliminate it. We use the simulation signal to demonstrate the performance of SVM and ICEEMDAN. The simulation data is x(t) given by

$$x(t) = 2\cos(8\pi t) + \cos(4\pi t) \tag{8}$$

where $x(t)$ is composed of two periodic functions. Fig. 4 illustrates time-domain waveforms, the horizontal axis represents the value range to $[-0.95, 0.95]$ and the vertical axis represents the signal's amplitude. There are 191 points in total. In the figure, the red curve is the envelope of the original signal from the value range $[-0.95, 0.95]$ and the blue is the real envelope. It

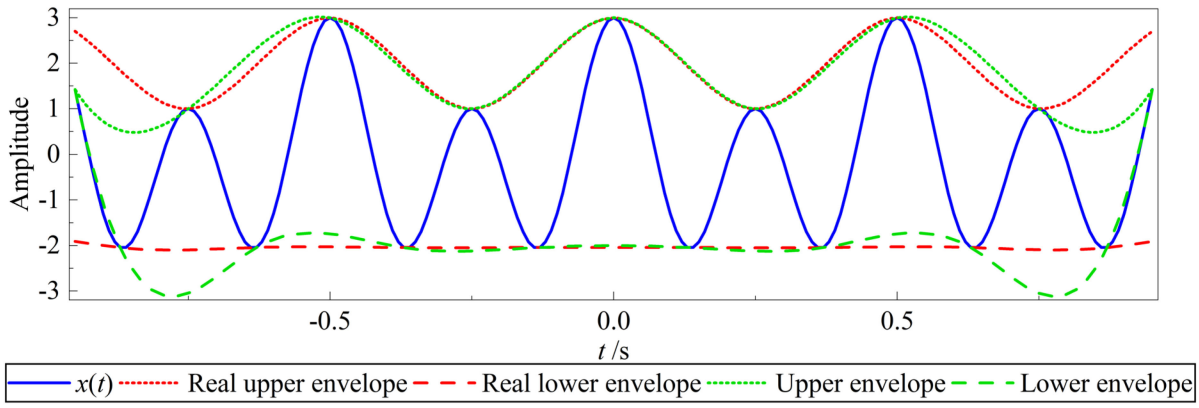

Fig. 4. Comparison of real envelopes and distorted envelopes of the simulation signal.

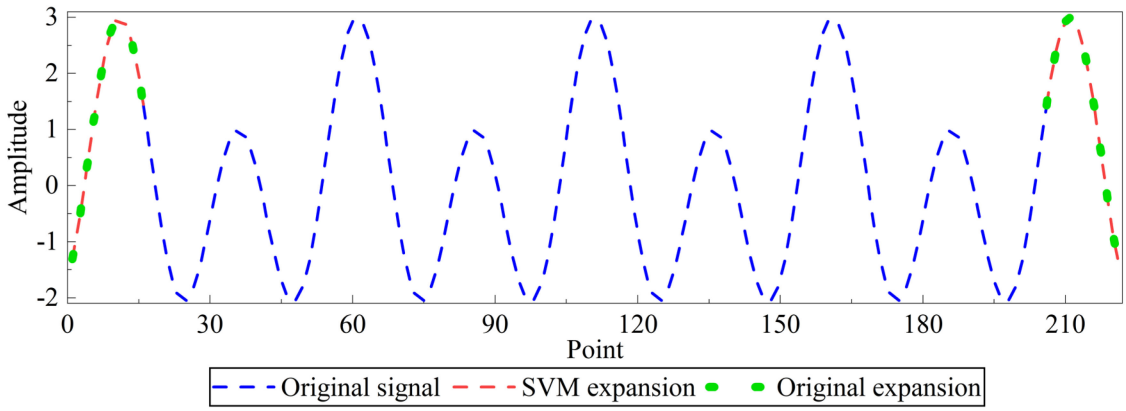

Fig. 5. Effect of the SVM on extending the simulation signal.

shows that the two endpoints of the signal are directly taken as the maximum and minimum points (green curve), but the endpoints are not extreme (red curve). The local extreme points are continuously reduced and sparse as the decomposition process progresses, and these false components gradually "pollute" the entire data inward. Because the data are distorted at both ends, the end effect is gradually generated. To eliminate or optimize the "end effect," it should start from the correction envelope to resolve, which requires that the left and right endpoints of the data cannot be taken as extreme points. So, it is necessary to predict the left and right endpoints to add extreme points.

The study used SVM to predict each end of the original signal by adding 15 points, for adding a certain number of extreme points and eliminating data distortion at both ends. As shown in Figs. 5 and 6, the horizontal axis is used as the length and the vertical axis is the amplitude. In Fig. 5, the SVM expansion data were extended 15 points at each side of the original signal, and the signal length after the expansion was 221. We obtain a correlation coefficient between the original expansion data and the SVM expansion data of 1, which demonstrates that the curves of the original expansion data and the SVM expansion data completely coincide, indicating an adequate prediction by the SVM. Fig. 6 demonstrates the two components of IMF1 and IMF2 obtained by ICEEMDAN decomposition of the original signal and SVM expansion data in Fig. 5. There is no mode mixing of the two components. IMF1 and IMF2 of the real signal are two trigonometric functions from $x(t)$, which are $2\cos(8\pi t)$ and $\cos(4\pi t)$, respectively. Using the real signal to demonstrate the results of the decomposition is more convincing. The result of the original data decomposition deviates at both ends. Moreover, this deviation has affected the internal data, but the extended data can attenuate this phenomenon.

Depending on the datasets (NDVI, precipitation, and temperature) length used in this article and the range of growing season, there are seven data points per year for a total of 34 years, so the length of each dataset includes 238 readings (seven periods in the growing season $\times$ 34 years). Using SVM to predict the datasets of a cycle at both ends of the long time series of NDVI, precipitation, and temperature, a cycle is the length of the growing season (seven points). The ICEEMDAN decomposes each predicted dataset that can not only reduce the end effect of the EMD family method itself but also eliminate the mode mixing. Different components of the original dataset can be obtained after decomposition, and then the frequency information of different components can be obtained by FFT

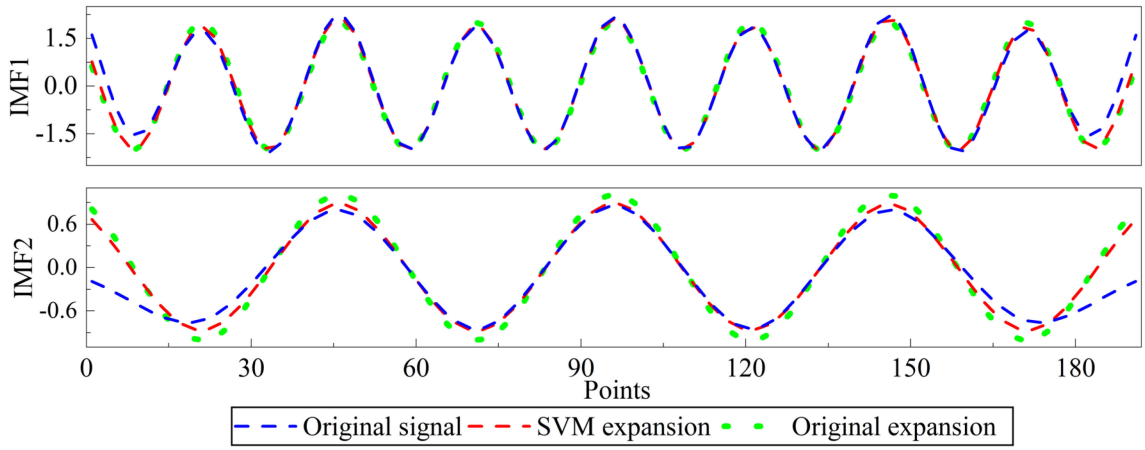

Fig. 6. Results of different data by ICEEMDAN.

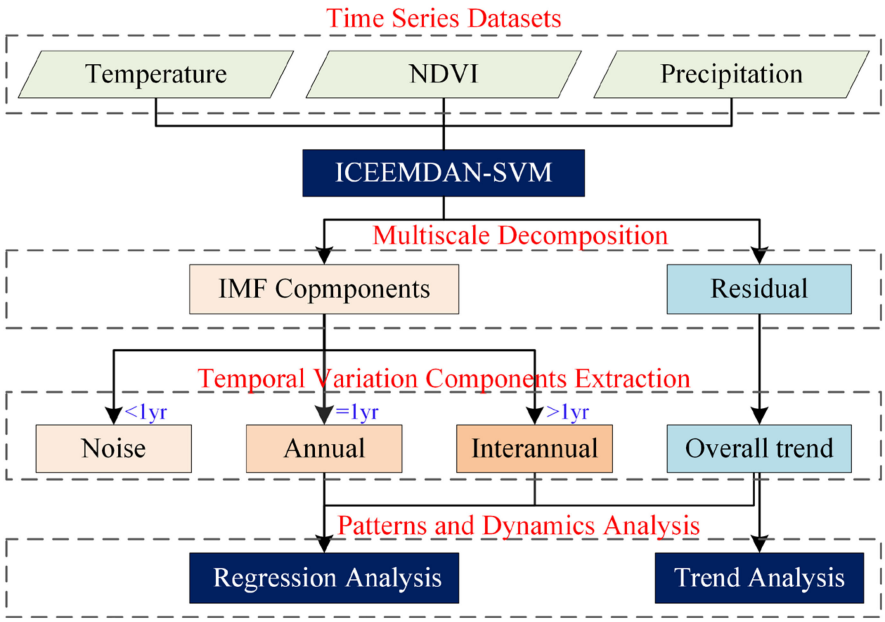

Fig. 7. Representation of the methodological framework used in this study.

[38], [50]. The sampling frequency is 7, and the sampling point is 238 for our study. After FFT, each point corresponds to a frequency point in hertz (Hz). When the main frequency of the obtained component is 1 Hz, it is divided into annual scales. The last component of the original data is the residual, which can represent the long-term trend, and the components between 1 Hz and residual are accumulated to be interannual scale. Therefore, the original datasets are divided into three scales, namely annual, interannual, and overall trend (see Fig. 7).

III. Results

A. Multiple Timescale Analysis for NDVI and Climate Factors by ICEEMDAN-SVM

The study used a multiscale decomposition method to decompose NDVI, precipitation, and temperature datasets to uncover the correlation between the vegetation index and climate variables at different timescales while discussing the vegetation cover change of the LP in the past 34 years. Fig. 8 shows the original data of NDVI, precipitation, and temperature during the growing season from 1982 to 2015. NDVI has clear periodicity, with some small fluctuations in the later stages. The change is complex and random, whereas the temperature has a stable periodicity. All three datasets show an upward trend, their long time series are nonstationary, and each data type has its characteristics. Therefore, when using ICEEMDAN to decompose different datasets based on pixels, different data should be added to different noises to reduce the mode mixing phenomenon. After many experiments, the number of white noise additions is 50, the standard noise deviation of temperature is 0.1, and the standard noise deviation of precipitation and NDVI is 0.3 [28], [76], [77].

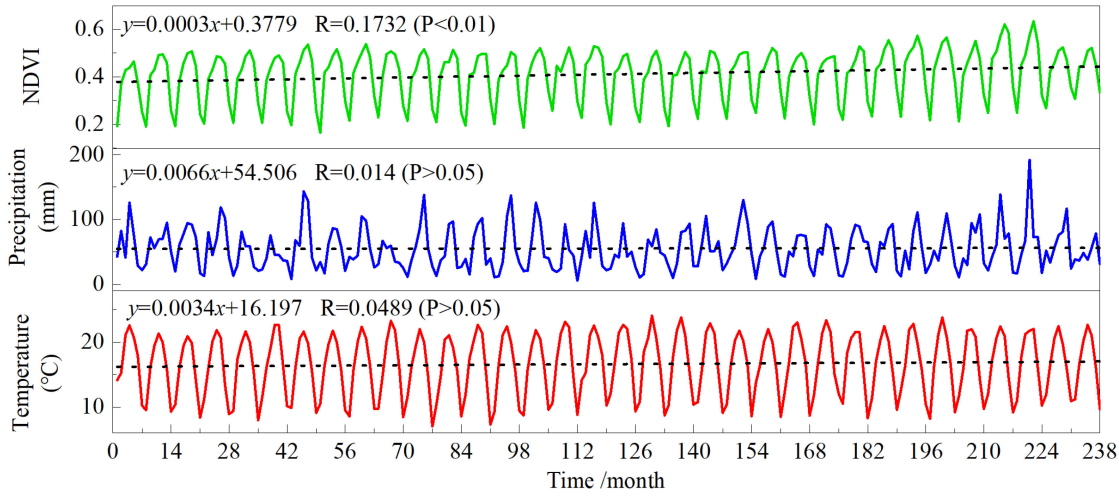

Fig. 8. Long time series of NDVI, precipitation, and temperature during the 1982–2015 growing season on the LP.

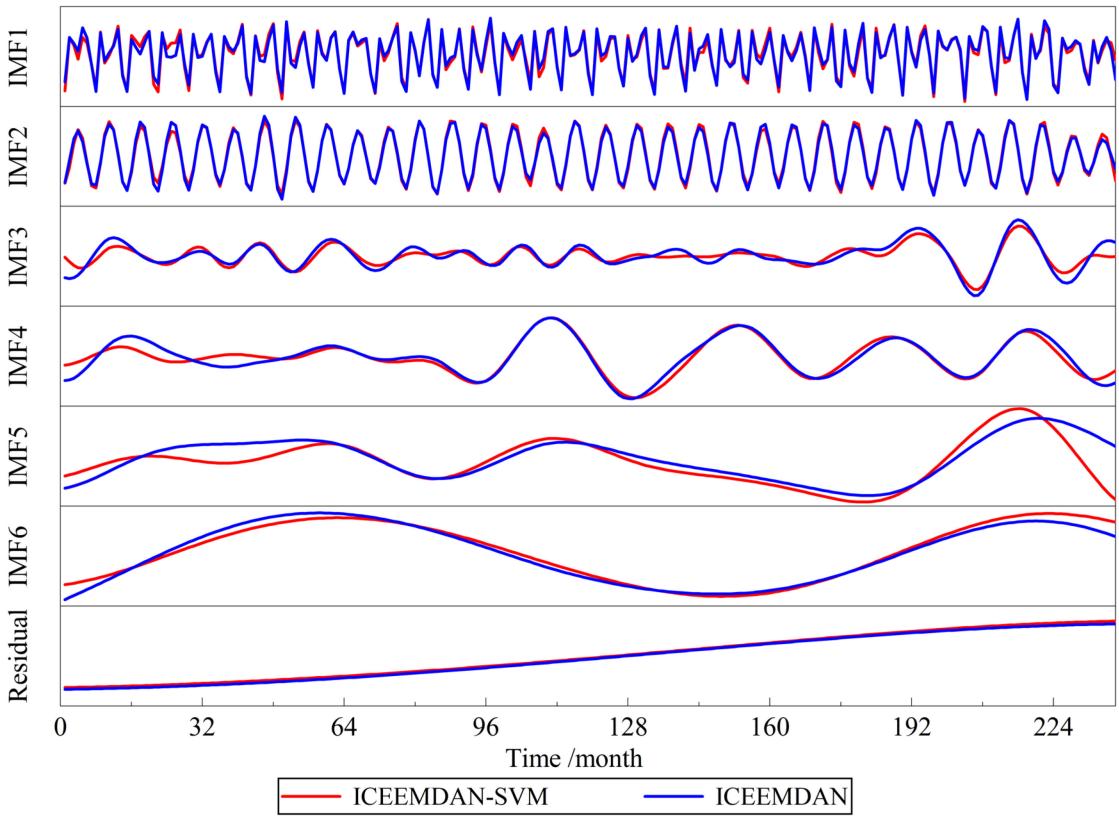

Fig. 9. Compare the NDVI decomposition results by the ICEEMDAN and the ICEEMDAN-SVM.

Due to the shortcomings of the EMD method, it can cause the issue of mode mixing and end effect. Therefore, it is essential to alleviate the end effect based on the SVM and ICEEMDAN method to eliminate the mode mixing phenomenon. Fig. 9 shows the results of NDVI decomposition by ICEEMDAN and ICEEMDAN-SVM. The ICEEMDAN decomposition of the data after SVM expansion can improve the end effect of the obtained component, and it is better to get the real change trend of each component than to perform the ICEEMDAN decomposition directly. The decomposition of the long time series of NDVI using EMD and ICEEMDAN-SVM is shown in Figs. 10 and 11, respectively, where, in Fig. 10(a), the horizontal axis indicates the length of NDVI and the vertical axis indicates the fluctuation range of NDVI values, and in Fig. 10(b), the horizontal axis indicates hertz and the vertical axis indicates the amplitude. IMF1 and IMF2 have mode mixing at the 1 Hz position in

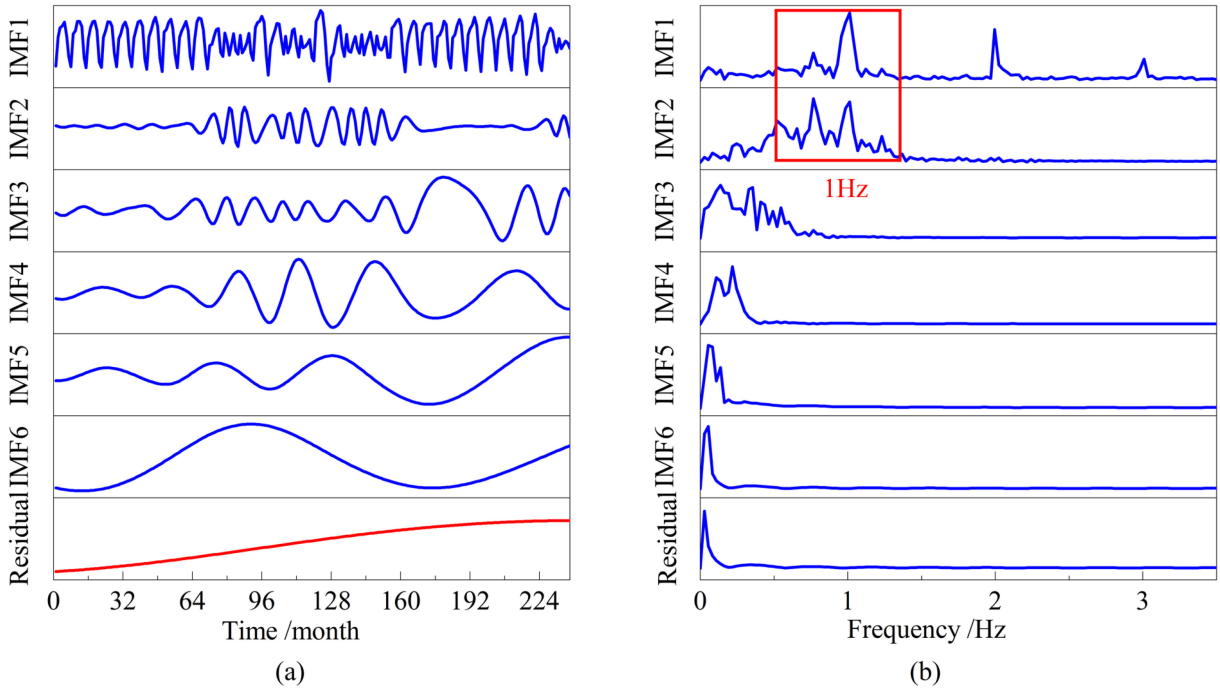

Fig. 10. (a) EMD decomposes the NDVI into six IMFs and a residual. (b) FFT spectrum of the seven components.

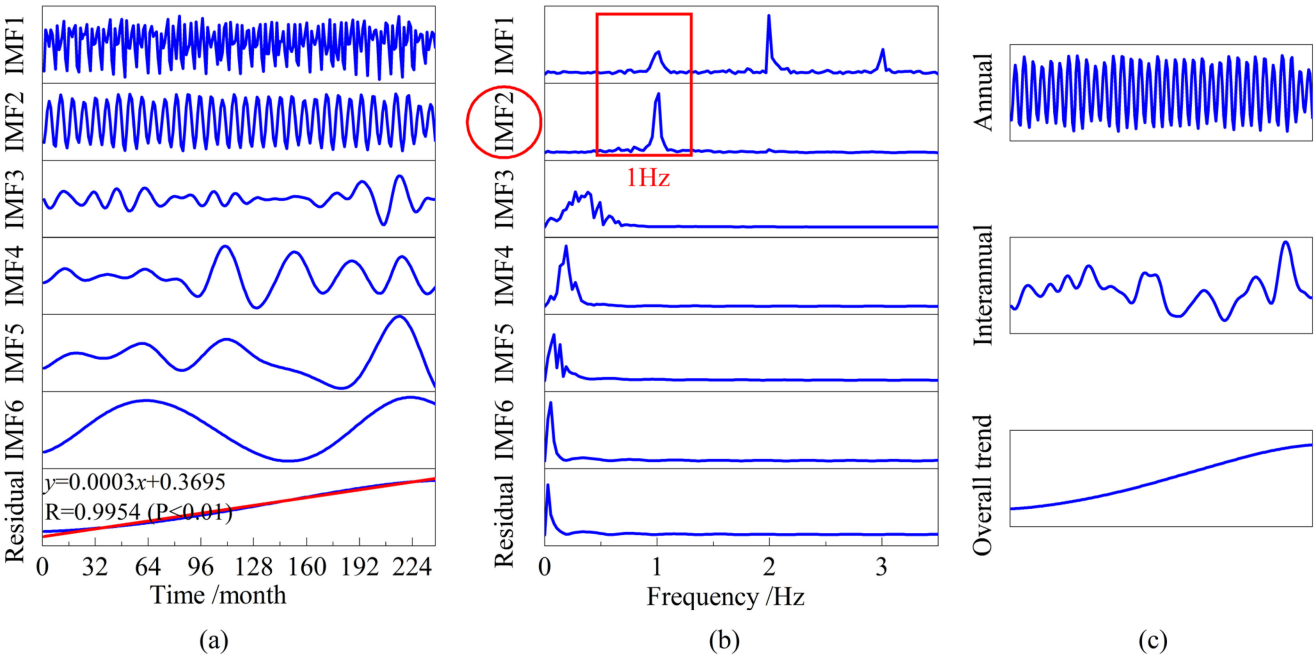

Fig. 11. Decompose long time series of the NDVI using the multiscale decomposition method. (a) ICEEMDAN-SVM decomposes the time series into six IMFs and a residual. (b) FFT spectrum of the seven components. (c) Dividing seven components into three scales, annual scale, interannual scale, and overall trend.

Fig. 10(b). Using the ICEEMDAN-SVM decomposed the NDVI in Fig. 11, the mode mixing of the components of IMF1 and IMF2 has been basically eliminated at the 1-Hz position.

In Fig. 11, ICEEMDAN-SVM decomposes the NDVI original time series into detailed information of different timescales. The noise and periodic fluctuation information can be obtained after decomposing the original data decomposition. The NDVI time series after multiscale decomposition is smoother, and the residual has an obvious increasing trend, which can more intuitively reflect the changing trend of vegetation coverage. NDVI is decomposed into six IMFS and a residual. According to the scale segmentation in this study, the first component of NDVI, IMF1 contains high-frequency changes as noise, IMF2 is the first scale as annual scale, and the four components of

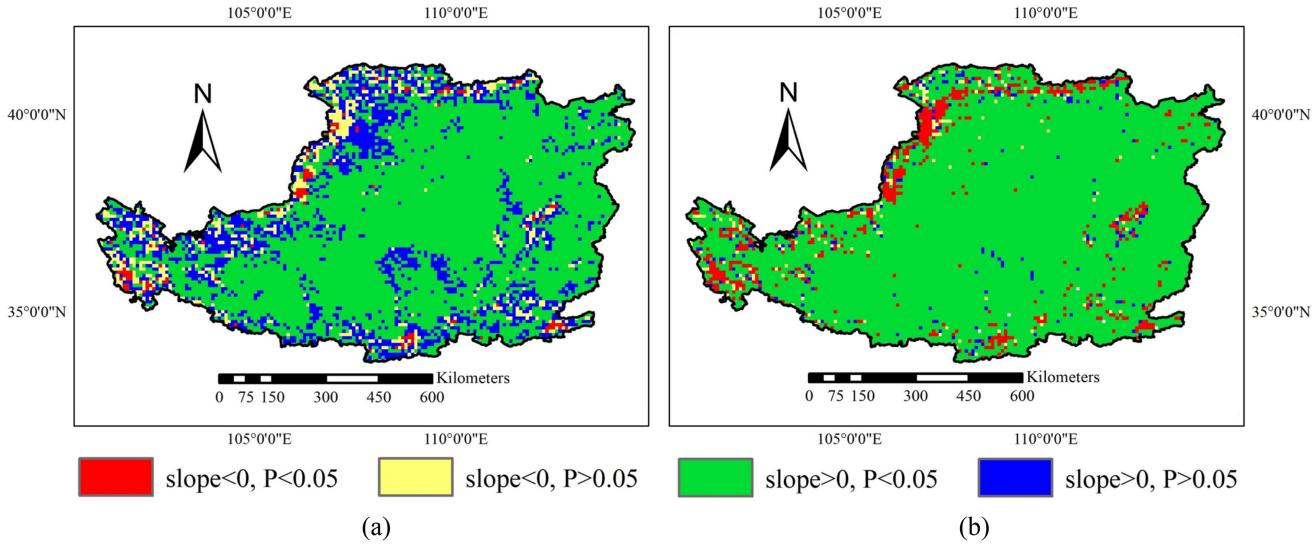

Fig. 12. Spatial change trends of NDVI between 1982 and 2015. (a) Original NDVI. (b) Residual NDVI.

IMF3-IMF6 are reorganized into the second scale as interannual scale, residual is the third scale as the overall trend. Similarly, the datasets of temperature and precipitation do the same processing at pixel scale to decompose based on the ICEEMDAN-SVM method.

B. Change Trends of Vegetation NDVI, Temperature, and Precipitation in the Loess Plateau (LP)

Studying the spatial distribution characteristics and change trend of the vegetation cover on LP from 1982 to 2015, using linear regression to study the changing trend, and the F test to analyze the significance level. The residual was obtained by decomposing the original data using the ICEEMDAN-SVM method, and then this study also conducted a trend analysis on the residual NDVI to verify whether it could express the long-term trend of the original data. The statistical results show that the changing trend of vegetation coverage mainly performed an increasing trend in the growing season. The percentage of areas with increasing trends of original NDVI was 91.23%, of which an extremely significant increase ($p < 0.01$) and significant increase ($p < 0.05$) accounted for 59.95% and 10.59%, respectively [see Fig. 12(a)]. In Fig. 12(b), the residual NDVI with an increasing trend is 91.16%, of which the proportions of areas showing an extremely significant increase and significant increase accounted for 87.89% and 0.98%, respectively. From the two results, it can be seen that the percentage of areas with an increasing trend of NDVI is much larger than the percentage of areas with decreasing trend. The proportion of area with significance in the residual NDVI change trend is greater than that in the original NDVI change trend, so the residual NDVI reflects the changing trend better than the original NDVI. All in all, the vegetation change in the LP area in the past 34 years has been dominated by improvement, with an increase in vegetation cover and an improved area larger than the degraded area.

TABLE III
MEAN VALUES OF GROWING-SEASON TOTAL PRECIPITATION (GSP), MEAN TEMPERATURE (GST), AND NDVI (GSN) OF DIFFERENT VEGETATION TYPES FROM 1982 TO 2015 ON THE LP

Label	GSN	GST (°C)	GSP (mm)
Study Area	0.41	16.60	387.05
AG	0.24	17.03	235.60
AB	0.11	17.37	201.68
SAF	0.71	17.99	438.72
SAG	0.35	15.64	377.61
SHF	0.75	17.80	496.48
SHG	0.49	14.20	420.88

The growing-season mean temperature (GST), NDVI (GSN), and growing-season total precipitation (GSP) are shown in Fig. 13, and the mean values of the study periods are shown in Table III. GSN and GST show a significant increasing trend, with increasing rates of 0.0018 year^{-1} and 0.0253 °C year^{-1} ($p < 0.01$), respectively, whereas GSP shows a slowly increasing trend (slope = 0.1983 mm year^{-1}, $p > 0.05$). Regarding the various trends of different vegetation types, there are significant spatial differences for GSP, GST, and GSN.

The average GSP in the study area from 1982 to 2015 was 387.05 mm. The GSP distribution has obvious regionality, and the vegetation types with the largest to smallest values of mean GSP are SHF > SAF > SHG > SAG > AG > AB. The mean GST during the study period is 16.60 °C. The vegetation type with the highest GST is SAF (17.99 °C), and the lowest average is SHG (14.20 °C). From the trend in Fig. 13(d) and Table III, the GST of different vegetation types shows a significant increasing trend with time, and there are certainly regional differences.

For GSN, it showed an apparent upward trend during the study period. In addition, the changing trend in GSN was significant for all vegetation types except for AB (slope = 0.0001 year^{-1}), and the changing trend of SAF was the most significant at 0.002

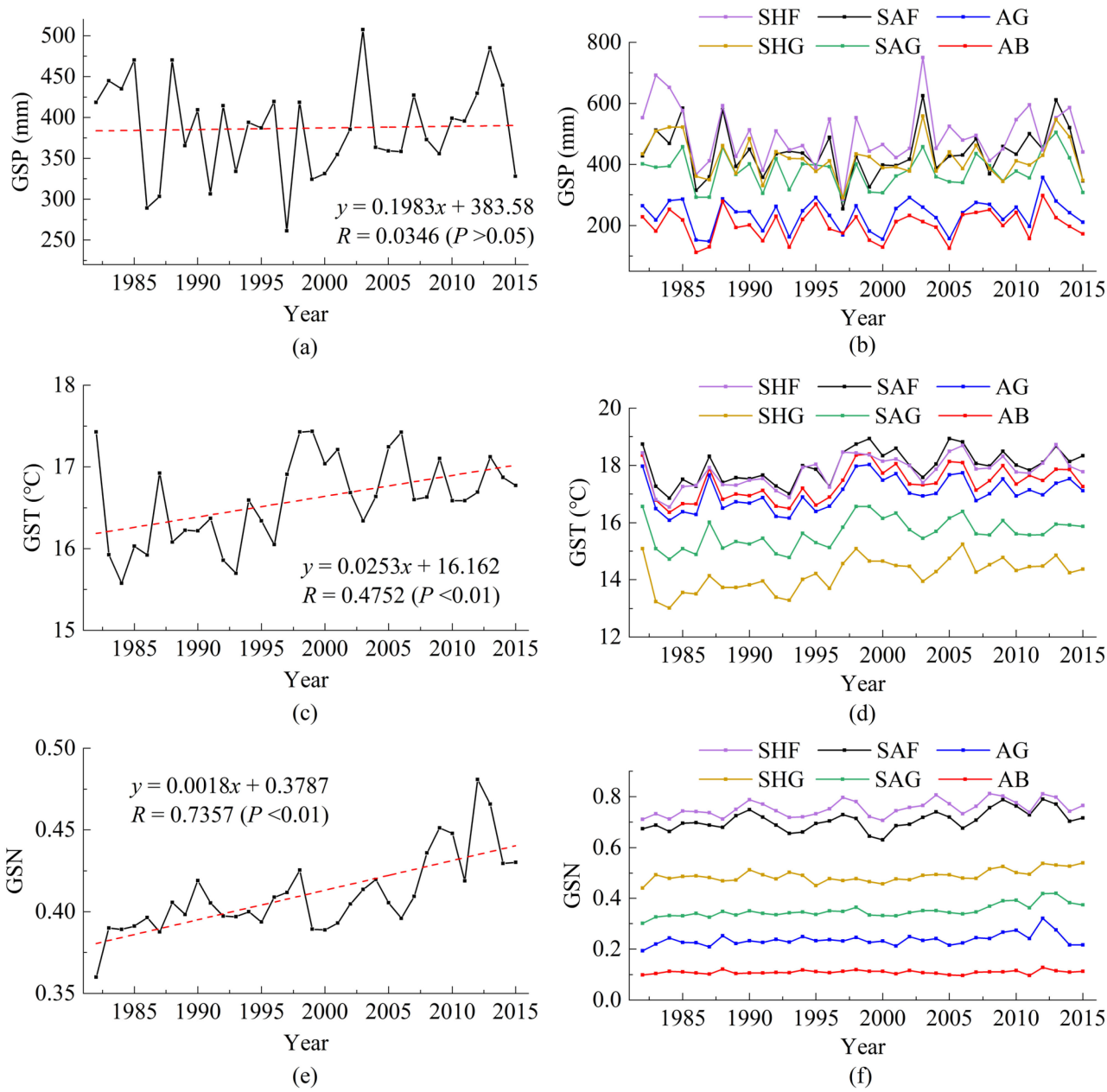

Fig. 13. Change trends of growing-season total precipitation (GSP), mean temperature (GST), and NDVI (GSN) from 1982 to 2015 on the LP.

year^{-1}. It indicates that the humid climate is more conducive to vegetation growth than the arid climate. The analysis of the three indicators shows that different climate regions have some effects on NDVI on LP, whereas there are some spatial differences in GSP and GST in different climate regions, which also have different degrees of influence on vegetation cover.

C. Relationships Between Vegetation and Climate Factors at Different Timescales

Our study used ICEEMDAN-SVM to divide the original datasets (NDVI, temperature, and precipitation) into annual scale, interannual scale, and overall trend to study the relative importance of climatic factors (temperature, precipitation) to NDVI. Partial correlation analysis was performed with temperature and precipitation as independent variables and NDVI as the dependent variable (see Fig. 14). Table IV shows the significant percentages of the area between climatic factors and NDVI at different timescales.

At the annual scale, the spatial characteristics of the partial correlation between the NDVI and temperature are illustrated in Fig. 14(a). The partial correlation coefficients have 97.29% of the study area passing the significance test ($p < 0.05$), and the percentage with significant positive correlation are 96.51%. Only a few vegetations had a nonsignificant negative correlation with temperature. The spatial characteristics of the partial correlation between NDVI and precipitation are illustrated in Fig. 14(b), 92.64% of the areas passed the significance test

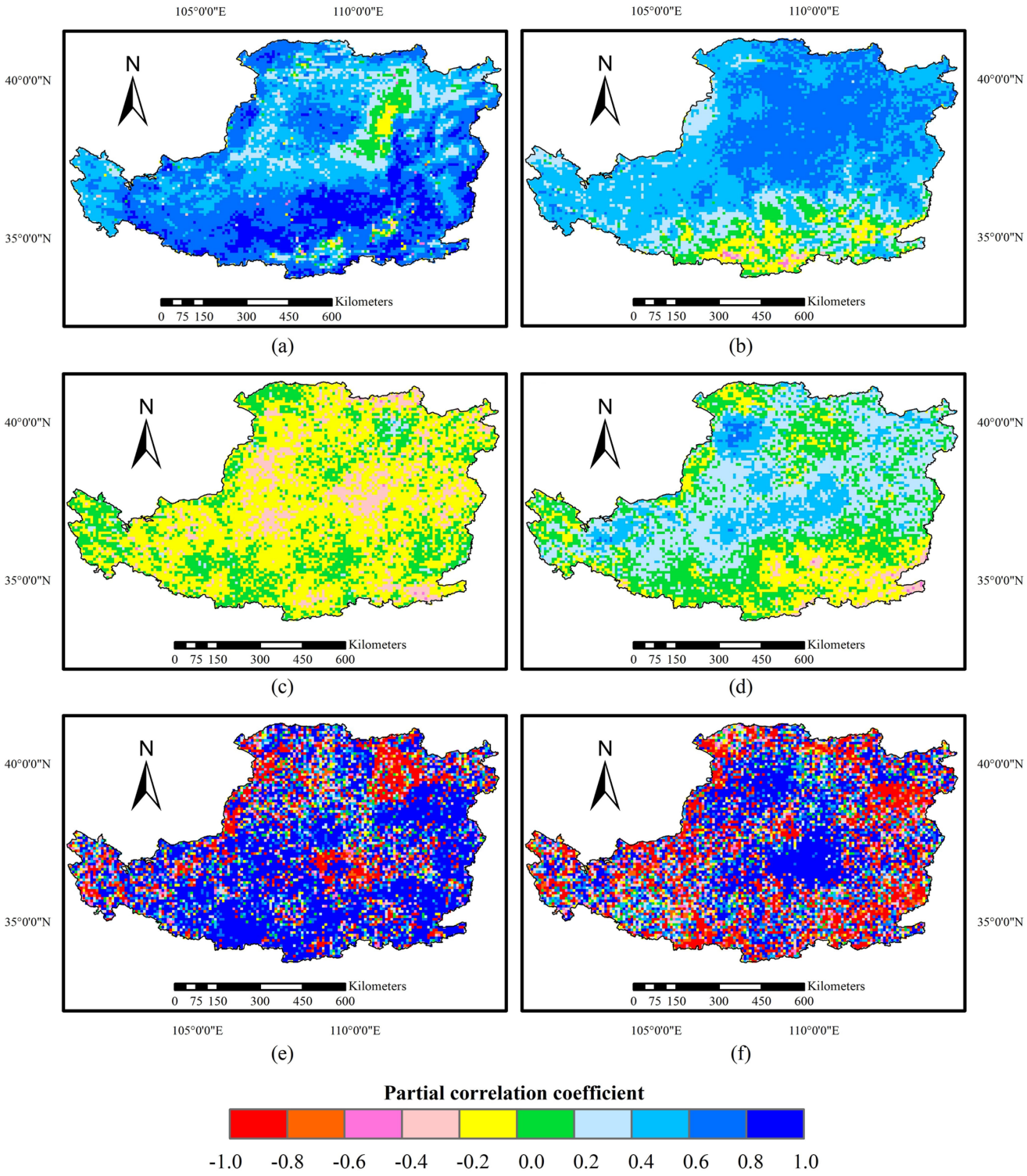

Fig. 14. Relationship between NDVI and climate factors (a), (c), and (e) represent the relationships with temperature, and (b), (d), and (f) represent the relationships with precipitation at the annual, interannual and overall trend, respectively.

($p < 0.05$), and the significant positive areas accounted for 90.24%, mainly located in arid and semiarid areas. The negatively correlated areas are primarily distributed in the semihumid areas. The overall effect of precipitation on vegetation changes in semiarid areas is greater than in arid areas. It shows that both precipitation and temperature have a powerful influence on vegetation coverage, and the temperature has a greater impact than precipitation on the annual scale.

At the interannual scale, the spatial characteristics of the partial correlation between NDVI and temperature are illustrated

TABLE IV
PERCENTAGE OF AREAS FOR DIFFERENT RELATIONSHIPS BETWEEN NDVI AND CLIMATIC FACTORS AT DIFFERENT TIMESCALES

	Annual		Interannual		Overall Trend	
	Temperature (AT)	Precipitation (AP)	Temperature (IT)	Precipitation (IP)	Temperature (OTT)	Precipitation (OTP)
$R<0, p<0.05$	0.78	2.40	35.56	6.98	27.22	41.15
$R<0, p>0.05$	0.87	3.43	36.52	11.48	2.13	2.54
$R>0, p>0.05$	1.84	3.93	21.73	17.25	2.32	2.51
$R>0, p<0.05$	96.51	90.24	6.19	64.29	68.33	53.80

in Fig. 14(c). In 72.08% of the areas, the temperature and NDVI are negatively correlated. Only 35.56% passed the significance test, with 6.19% of the regions where the temperature was positively correlated with NDVI. The spatial characteristics of the partial correlation between NDVI and precipitation are illustrated in Fig. 14(d). The partial correlation coefficients between precipitation and NDVI have 71.27% of the areas that passed the significance test. The areas with a positive correlation are 64.29%, generally located in the central LP, containing the semiarid areas. The negative correlation (6.98%) is primarily distributed in the upper reaches of the Yellow River and semihumid regions. Therefore, it can be explained that vegetation coverages have less demand for precipitation when the soil moisture is relatively high. In addition, the explanatory power of the effect of temperature and precipitation on vegetation cover change is weaker than that of the annual scale.

In the overall trend, the spatial characteristics of the partial correlation between vegetation NDVI and temperature are illustrated in Fig. 13(e). The positive areas were 68.33%, the negative areas were 27.22% ($p < 0.05$). The spatial characteristics of the partial correlation between NDVI and precipitation are illustrated in Fig. 14(f). The partial correlation coefficients between precipitation and NDVI passed the significance test, in 94.95% of the areas, with 53.80% ($p < 0.05$) of the regions showing a significant positive correlation. It can be seen from the above analysis that the change of NDVI is influenced by both temperature and precipitation, and different regions and climates have different influences on vegetation coverage. On different timescales, the response of vegetation to precipitation and temperature is different. The above analysis results can show that precipitation and temperature can better explain the changes in vegetation coverages on the annual scale and the overall trend, which is greater than the interannual scale.

This article analyzed the correlation between different vegetation types and climatic factors at different timescales, and the correlation coefficients of pixels of different vegetation types were statistically analyzed. As can be seen in Fig. 15, the same vegetation responds differently to temperature and precipitation on different timescales. At the same timescale, the same climatic factors have different effects on different vegetation types. Fig. 15(a) illustrates the distribution of the correlation coefficients of AB for annual scale, interannual scale, and overall trend with precipitation and temperature. On the annual scale, the influence of temperature on AB is greater than that of precipitation, and the mean values of the absolute values of the partial correlation coefficients ($|R|_{\text{mean}}$) are 0.53 and 0.47 ($p < 0.05$), respectively. For the interannual scale, precipitation has a greater impact on it than temperature. On the overall trend, precipitation and temperature have similar effects on AB.

Fig. 15(b), (d), and (f) shows the partial correlation coefficients of grassland in arid, semiarid, and semihumid regions with precipitation and temperature at different scales. For the annual scale, the correlation between Grassland and precipitation in the semiarid region is the strongest, with the $|R|_{\text{mean}}$ being 0.57 ($p < 0.05$), and the semihumid region ($|R|_{\text{mean}} = 0.35$) is the weakest, indicating that precipitation exists a little effect on vegetation in the semihumid region. The temperature exists the strongest impact on Grassland in the semihumid region ($|R|_{\text{mean}} = 0.77$), and the arid region ($|R|_{\text{mean}} = 0.50$) is the weakest impact. This indicates that temperature has an inhibitory effect on vegetation in arid areas. For the overall trend, the effect of precipitation on Grassland is greater than that of temperature.

Mixed forests are mainly distributed in semiarid and semihumid climate regions. As shown in Fig. 15(c) and (e), at the annual scale, the impact of precipitation on SAF ($|R|_{\text{mean}} = 0.44$) is higher than SHF ($|R|_{\text{mean}} = 0.15$). There is no obvious difference in the effect of temperature on mixed forests in different climate regions. The effect of temperature on mixed forests is higher than that of precipitation. Similarly, at the interannual scale, the effect of precipitation and temperature on mixed forests is weaker. For the overall trend, for SAF, both precipitation and temperature correlate well, but for SHF, the effect of temperature ($|R|_{\text{mean}} = 0.86$) is higher than that of precipitation ($|R|_{\text{mean}} = 0.72$). It showed a higher correlation compared to the annual and interannual scales.

In general, at the annual scale, the impact of precipitation on different vegetation types is SAG > AG > AB > SAF > SHG > SHF, and the effect of temperature on different vegetation types is SHF > SAF > SHG > SAG > AB > AG. At the interannual scale, the effect of precipitation on different vegetation types is AG > SAG >AB > SHF > SAF > SHG, and the impact of temperature on different vegetation types is AG > SAG > AB> SHG > SAF > SHF. For overall trend, the effect of precipitation on different vegetation types is AG > AB > SAF > SAG > SHF > SHG, and the effect of temperature on different vegetation types is SHF > SHG > SAF > AB > SAG > AG. Therefore, at different timescales, precipitation has a greater impact on vegetation coverage in arid and semiarid regions. The temperature has a greater effect on vegetation coverage in the semihumid region, and the impact on mixed forests is higher than that on Grasslands.

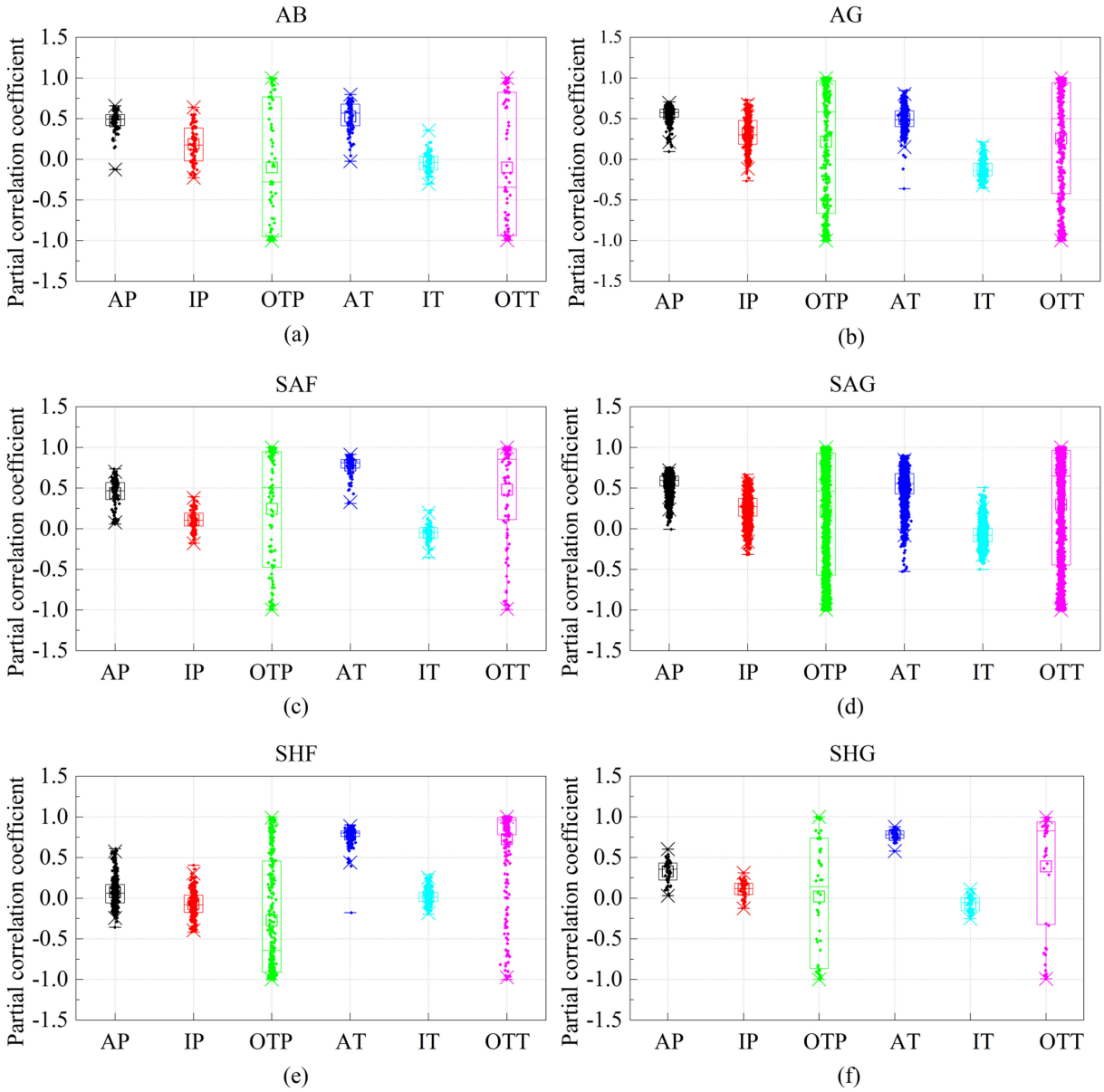

Fig. 15. Partial correlation coefficients of different vegetations with temperature and precipitation at different timescales.

IV. Discussions

A. Methodological Considerations and Innovations

The ICEEMDAN method is a time-frequency analysis method in the field of signals, which is used in this article to study the relationship between vegetation dynamics and climate change. As an extension of the EMD method, ICEEMDAN can obtain components with less noise and stronger physical meaning [36], [43], which largely eliminates the problem of mode mixing [28]. However, the ICEEMDAN method produces endpoint effects in the decomposition, which is a problem with the EMD family [40]–[42]. When time series are decomposed directly using ICEEMDAN, both endpoints of the original data are mistaken for extreme values. Therefore, the false information will gradually "pollute" the entire data inward, causing the information at two endpoints of each component to be distorted. Using SVM to predict the changing trend of long time series in many fields, and previous studies considered that the SVM has favorable generalization ability and high prediction accuracy [44]. Cheng et al. [40] and Yang et al. [48] used the SVM to expand the original time series at the two endpoints to reduce the endpoint problem of the EMD method and achieved excellent results. Our study also proves that SVM can predict extending the original data before decomposition, which reduces the end effect on each component.

B. Spatial and Temporal Variation of NDVI, Temperature, and Precipitation in the Loess Plateau (LP)

The study used the ICEEMDAN-SVM method to strip out the residual of the long time series to study the spatial and temporal trends of vegetation on the LP from 1982 to 2015. Previous

studies pointed out that the residual component can represent the overall trend of the original time series [35], [36], [78], so it can justify the study in this article. The study showed that the spatial trend of vegetation mainly increased on LP from 1982 to 2015. Related studies also show that vegetation cover of the LP has had an increasing trend in recent years [63], [79], [80], which is identical to our findings. Meanwhile, the residual NDVI change trend is more significant (95.84%, $p < 0.05$) than the original NDVI (72.24%), $p < 0.05$). Therefore, the residual NDVI can reflect the changes in vegetation well. The above results support the conclusion that vegetation activity has increased significantly in the northern hemisphere at middle and high latitudes [81]–[83]. Spatially, the LP region straddles three climatic zones, arid, semiarid, and semihumid, and has obvious environmental characteristics of ecological transition zones (see Fig. 1).

The study analyzed precipitation, temperature, and NDVI according to six vegetation types (see Table II), and the results showed that NDVI, temperature, and precipitation under different climatic zones in the LP region had significant differences in the past 34 years. It has been shown that climatic zones can influence the growth of vegetation [84], [85]. Overall, our results further reveal the spatial and temporal changes in vegetation dynamics and climate in the LP over the past 34 years.

C. Effects of Climate Change on Vegetation NDVI Changes at Multitimescale

There are different effects of different climatic factors on the same vegetation, and there are also different responses of different vegetation to the same climatic factors [69], [86], [87]. Using the ICEEMDAN-SVM method can divide long time series (NDVI, temperature, and precipitation) into annual scale, interannual scale, and overall trend and use regression analysis to study the relationship between climatic factors and NDVI at different timescales. The research uncovered that the relationship between vegetation cover and climatic factors is not only influenced by climatic and vegetation types but also changes with timescales [88]–[90]. The effects of temperature and precipitation on NDVI are different at different timescales [16], [91], [92]. NDVI correlates more with temperature and precipitation on the annual scale and overall trend than on the interannual scale. At the annual scale, the correlation between precipitation and NDVI ($|R|_{\mathrm{mean}} = 0.51, p < 0.05$) is lower than the correlation between temperature and NDVI ($|R|_{\mathrm{mean}} = 0.60$, $p < 0.05$), and the relationship between precipitation and temperature on vegetation coverage is mainly positive, which is consistent with the study of Zhang et al. [90]. At the interannual scale, the correlation between precipitation and NDVI ($|R|_{\mathrm{mean}} = 0.29$, $p < 0.05$) is higher than the correlation between temperature and NDVI ($|R|_{\mathrm{mean}} = 0.19, p < 0.05$), and the effect of precipitation on vegetation is mainly positively correlated, and the temperature is mainly negatively correlated. For the overall trend, the correlation between precipitation and NDVI ($|R|_{\mathrm{mean}} = 0.75$, $p < 0.05$) is lower than the correlation between temperature and NDVI ($|R|_{\mathrm{mean}} = 0.80$, $p < 0.05$), and temperature promotes vegetation growth more than precipitation. Therefore, long-term precipitation increases will prevent vegetation changes, and long-term temperature increases can promote photosynthesis, which is further beneficial to vegetation changes [36], [88], [94].

This article showed the correlation between different vegetation types in different climate regions and climatic factors at different timescales have obvious differences. Overall, vegetation in arid and semiarid regions requires higher precipitation than temperature [95]–[98]. However, this relationship has less impact in semihumid regions [18], [36], [64]. The temperature is the main driving factor for vegetation in semihumid regions, which is also consistent with previous studies [94], [99]. At different timescales, precipitation has greater changes in vegetation coverages in arid and semiarid regions, and the effect of precipitation on Grassland is greater than that of Mixed forests. The temperature has a greater effect on vegetation coverages in semihumid regions, and the impact on Mixed forests is higher than that on Grasslands. Most studies have shown that NDVI has no significant correlation with temperature and precipitation in most areas. Although, only the interannual scale showed that most areas were insignificant on the LP in our study. As the timescale increases, the effect of climate change on vegetation becomes stronger. It shows that climatic factors are the major factors that affect long-term vegetation changes [36], [38].

V. Conclusion

Taking the LP as an example, this article innovatively integrates ICEEMDAN and SVM methods to study the relationship between vegetation dynamics and climate change at different timescales. The main findings are as follows:

1) Compared to the EMD method, the ICEEMDAN method can reduce the effects of mode mixing, and the use of SVM can suppress the effects of the end effect before decomposition.
2) ICEEMDAN-SVM was used to separate the long-time series of vegetation and climate change on the LP from 1982 to 2015 into three scales, annual, interannual, and overall trend, where NDVI under the overall trend scale can symbolize the overall trend of the original data.
3) The vegetation indices and climate factors show significant spatial and temporal differences under different climate zones.
4) The relationship between vegetation dynamics and climate change showed significant variability at different timescales, where overall trend $>$ annual $>$ interannual. Under the same timescale, different climatic factors have different effects on the same vegetation, and different vegetations have different responses on the same climatic factors.

The study proved that the climatic zone of the LP also had an impact on the study results. Overall, vegetation types in arid and semiarid regions have a greater demand for precipitation, and temperature is the major driving factor for vegetation in a semihumid climate. This study reveals the nonlinear characteristics of vegetation change and its relationship with the drivers in the LP. The patterns and dynamics of ICEEMDAN-SVM are significant for further use in ecosystem research in other regions, which can reveal some hidden information to better understand the dynamic

changes of fragile ecosystems and is important for the research of vegetation conservation and fragile ecosystem restoration under global climate change. Since this study does not consider the nonlinear effects of human activities and other natural factors, further work should gather more influencing factors for multiple timescale analysis to ascertain the influences of other factors on vegetation cover to conduct a more comprehensive analysis.

REFERENCES

[1] T. W. Dahl and S. K. Arens, "The impacts of land plant evolution on Earth's climate and oxygenation state – An interdisciplinary review," *Chem. Geol.*, vol. 547, 2020, Art. no. 119665.

[2] X. Feng et al., "Revegetation in China's Loess Plateau is approaching sustainable water resource limits," *Nat. Climate Change*, vol. 6, no. 11, pp. 1019–1022, 2016.

[3] P. Bousquet, P. Peylin, P. Ciais, C. L. Quéré, P. Friedlingstein, and P. P. Tans, "Regional changes in carbon dioxide fluxes of land and oceans since 1980," *Science*, vol. 290, no. 5495, pp. 1342–1346, 2000.

[4] D. Baldocchi et al., "FLUXNET: A new tool to study the temporal and spatial variability of ecosystem-scale carbon dioxide, water vapor, and energy flux densities," *Bull. Amer. Meteorol. Soc.*, vol. 82, no. 11, pp. 2415–2434, 2001.

[5] K. M. de Beurs and G. M. Henebry, "A statistical framework for the analysis of long image time series," *Int. J. Remote Sens.*, vol. 26, no. 8, pp. 1551–1573, 2005.

[6] M. Zhang et al., "Nonlinear characteristics of the vegetation change and its response to climate change in the karst region of southwest China," *Prog. Phys. Geogr., Earth Environ.*, vol. 46, no. 4, pp. 497–514, 2021.

[7] W. J. Burroughs, *Weather Cycles: Real Or Imaginary?* Cambridge, U.K.: Cambridge Univ. Press, 2003.

[8] M. D. Schwartz, "Advancing to full bloom: Planning phenological research for the 21st century," *Int. J. Biometeorol.*, vol. 42, no. 3, pp. 113–118, 1999.

[9] J. Verbesselt, R. Hyndman, G. Newnham, and D. Culvenor, "Detecting trend and seasonal changes in satellite image time series," *Remote Sens. Environ.*, vol. 114, no. 1, pp. 106–115, 2010.

[10] B. C. Reed, J. F. Brown, D. VanderZee, T. R. Loveland, J. W. Merchant, and D. O. Ohlen, "Measuring phenological variability from satellite imagery," *J. Vegetation Sci.*, vol. 5, no. 5, pp. 703–714, 1994.

[11] B. Martínez and M. A. Gilabert, "Vegetation dynamics from NDVI time series analysis using the wavelet transform," *Remote Sens. Environ.*, vol. 113, no. 9, pp. 1823–1842, 2009.

[12] Q. Sun, C. Liu, T. Chen, and A. Zhang, "A weighted-time-lag method to detect lag vegetation response to climate variation: A case study in Loess Plateau, China, 1982–2013," *Remote Sens.*, vol. 13, no. 5, 2021, Art. no. 923.

[13] J. Krishnaswamy, R. John, and S. Joseph, "Consistent response of vegetation dynamics to recent climate change in tropical mountain regions," *Glob. Change Biol.*, vol. 20, no. 1, pp. 203–215, 2014.

[14] J. Fang, S. Piao, Z. Tang, C. Peng, and W. Ji, "Interannual variability in net primary production and precipitation," *Science*, vol. 293, no. 5536, pp. 1723–1723, 2001.

[15] C. S. Neigh, C. J. Tucker, and J. R. Townshend, "North American vegetation dynamics observed with multi-resolution satellite data," *Remote Sens. Environ.*, vol. 112, no. 4, pp. 1749–1772, 2008.

[16] G. Bao, Y. Bao, Z. Qin, Y. Zhou, and A. Shiirev, "Vegetation cover changes in Mongolian Plateau and its response to seasonal climate changes in recent 10 years," *Sci. Geogr. Sin.*, vol. 33, no. 5, pp. 613–621, 2013.

[17] B. Chen et al., "Changes in vegetation photosynthetic activity trends across the Asia–Pacific region over the last three decades," *Remote Sens. Environ.*, vol. 144, pp. 28–41, 2014.

[18] K. Rishmawi, S. D. Prince, and Y. Xue, "Vegetation responses to climate variability in the northern arid to sub-humid zones of sub-Saharan Africa," *Remote Sens.*, vol. 8, no. 11, 2016, Art. no. 910.

[19] E. L. Bunting, S. M. Munson, and M. L. Villarreal, "Climate legacy and lag effects on dryland plant communities in the southwestern U.S.," *Ecol. Indicators*, vol. 74, pp. 216–229, 2017.

[20] R. Stöckli and P. L. Vidale, "European plant phenology and climate as seen in a 20-year AVHRR land-surface parameter dataset," *Int. J. Remote Sens.*, vol. 25, no. 17, pp. 3303–3330, 2004.

[21] M. E. Jakubauskas, D. R. Legates, and J. H. Kastens, "Harmonic analysis of time-series AVHRR NDVI data," *Photogrammetric Eng. Remote Sens.*, vol. 67, no. 4, pp. 461–470, 2001.

[22] S. Azzali and M. Menenti, "Mapping vegetation-soil-climate complexes in southern Africa using temporal Fourier analysis of NOAA-AVHRR NDVI data," *Int. J. Remote Sens.*, vol. 21, no. 5, pp. 973–996, 2000.

[23] T. Sakamoto, M. Yokozawa, H. Toritani, M. Shibayama, N. Ishitsuka, and H. Ohno, "A crop phenology detection method using time-series MODIS data," *Remote Sens. Environ.*, vol. 96, no. 3/4, pp. 366–374, 2005.

[24] C. Torrence and G. P. Compo, "A practical guide to wavelet analysis," *Bull. Amer. Meteorol. Soc.*, vol. 79, no. 1, pp. 61–78, 1998.

[25] M. Farge, "Wavelet transforms and their applications to turbulence," *Annu. Rev. Fluid Mech.*, vol. 24, no. 1, pp. 395–458, 1992.

[26] D. B. Percival, M. Wang, and J. E. Overland, "An introduction to wavelet analysis with applications to vegetation time series," *Community Ecol.*, vol. 5, no. 1, pp. 19–30, 2004.

[27] P. Jonsson and L. Eklundh, "Seasonality extraction by function fitting to time-series of satellite sensor data," *IEEE Trans. Geosci. Remote Sens.*, vol. 40, no. 8, pp. 1824–1832, Aug. 2002.

[28] P. Hawinkel, E. Swinnen, S. Lhermitte, B. Verbist, J. Van Orshoven, and B. Muys, "A time series processing tool to extract climate-driven interannual vegetation dynamics using ensemble empirical mode decomposition (EEMD)," *Remote Sens. Environ.*, vol. 169, pp. 375–389, 2015.

[29] G. L. Galford, J. F. Mustard, J. Melillo, A. Gendrin, C. C. Cerri, and C. E. Cerri, "Wavelet analysis of MODIS time series to detect expansion and intensification of row-crop agriculture in Brazil," *Remote Sens. Environ.*, vol. 112, no. 2, pp. 576–587, 2008.

[30] Z. Wu, E. K. Schneider, B. P. Kirtman, E. S. Sarachik, N. E. Huang, and C. J. Tucker, "The modulated annual cycle: An alternative reference frame for climate anomalies," *Climate Dyn.*, vol. 31, no. 7, pp. 823–841, 2008.

[31] C.-Y. Chang, J. C. H. Chiang, M. F. Wehner, A. R. Friedman, and R. Ruedy, "Sulfate aerosol control of tropical Atlantic climate over the twentieth century," *J. Climate*, vol. 24, no. 10, pp. 2540–2555, 2011.

[32] A. C. Yang, S.-J. Tsai, and N. E. Huang, "Decomposing the association of completed suicide with air pollution, weather, and unemployment data at different time scales," *J. Affect. Disord.*, vol. 129, no. 1–3, pp. 275–281, 2011.

[33] Y. Kong, Y. Meng, W. Li, A. Yue, and Y. Yuan, "Satellite image time series decomposition based on EEMD," *Remote Sens.*, vol. 7, no. 11, pp. 15583–15604, 2015.

[34] R. Verma and S. Dutta, "Vegetation dynamics from denoised NDVI using empirical mode decomposition," *J. Indian Soc. Remote Sens.*, vol. 41, no. 3, pp. 555–566, 2013.

[35] T. Chen et al., "Trend analysis of relationship between primary productivity, precipitation and temperature in Inner Mongolia," *ISPRS Int. J. Geo-Inf.*, vol. 7, no. 6, 2018, Art. no. 214.

[36] X. Qi, J. Jia, H. Liu, and Z. Lin, "Relative importance of climate change and human activities for vegetation changes on China's silk road economic belt over multiple timescales," *Catena*, vol. 180, pp. 224–237, 2019.

[37] W. Zhang, L. Wang, F. Xiang, W. Qin, and W. Jiang, "Vegetation dynamics and the relations with climate change at multiple time scales in the Yangtze River and Yellow River Basin, China," *Ecol. Indicators*, vol. 110, 2020, Art. no. 105892.

[38] X. Liu, Z. Tian, A. Zhang, A. Zhao, and H. Liu, "Impacts of climate on spatiotemporal variations in vegetation NDVI from 1982–2015 in Inner Mongolia, China," *Sustainability*, vol. 11, no. 3, 2019, Art. no. 768.

[39] N. E. Huang et al., "The empirical mode decomposition and the Hilbert spectrum for nonlinear and non-stationary time series analysis," *Proc. Roy. Soc. A Math. Phys. Eng. Sci.*, vol. 454, no. 1971, pp. 903–995, 1998.

[40] J. Cheng, D. Yu, and Y. Yang, "Application of support vector regression machines to the processing of end effects of Hilbert–Huang transform," *Mech. Syst. Signal Process.*, vol. 21, no. 3, pp. 1197–1211, 2007.

[41] Y. Deng, W. Wang, C. Qian, Z. Wang, and D. Dai, "Boundary-processing-technique in EMD method and Hilbert transform," *Chin. Sci. Bull.*, vol. 46, no. 11, pp. 954–960, 2001.

[42] F. Wu and L. Qu, "An improved method for restraining the end effect in empirical mode decomposition and its applications to the fault diagnosis of large rotating machinery," *J. Sound Vib.*, vol. 314, no. 3–5, pp. 586–602, 2008.

[43] M. A. Colominas, G. Schlotthauer, and M. E. Torres, "Improved complete ensemble EMD: A suitable tool for biomedical signal processing," *Biomed. Signal Process. Control*, vol. 14, pp. 19–29, 2014.

[44] S. Huang, J. Chang, Q. Huang, and Y. Chen, "Monthly streamflow prediction using modified EMD-based support vector machine," *J. Hydrol.*, vol. 511, pp. 764–775, 2014.

[45] D.-C. Lin, Z.-L. Guo, F.-P. An, and F.-L. Zeng, "Elimination of end effects in empirical mode decomposition by mirror image coupled with support vector regression," *Mech. Syst. Signal Process.*, vol. 31, pp. 13–28, 2012.

[46] G. Mountrakis, J. Im, and C. Ogole, "Support vector machines in remote sensing: A review," *ISPRS J. Photogrammetry Remote Sens.*, vol. 66, no. 3, pp. 247–259, 2011.

[47] J. Wang, W. Liu, and S. Zhang, "An approach to eliminating end effects of EMD through mirror extension coupled with support vector machine method," *Pers. Ubiquitous Comput.*, vol. 23, no. 3, pp. 443–452, 2019.

[48] J. Yang, P. Li, Y. Yang, and D. Xu, "An improved EMD method for modal identification and a combined static-dynamic method for damage detection," *J. Sound Vib.*, vol. 420, pp. 242–260, 2018.

[49] M. Menenti, S. Azzali, W. Verhoef, and R. van Swol, "Mapping agroecological zones and time lag in vegetation growth by means of Fourier analysis of time series of NDVI images," *Adv. Space Res.*, vol. 13, no. 5, pp. 233–237, 1993.

[50] J. W. Cooley and J. W. Tukey, "An algorithm for the machine calculation of complex Fourier series," *Math. Comput.*, vol. 19, no. 90, pp. 297–301, 1965.

[51] Y. Wang, M. Shao, Y. Zhu, and Z. Liu, "Impacts of land use and plant characteristics on dried soil layers in different climatic regions on the Loess Plateau of China," *Agricultural Forest Meteorol.*, vol. 151, no. 4, pp. 437–448, 2011.

[52] C. H. Lu, M. K. van Ittersum, and R. Rabbinge, "A scenario exploration of strategic land use options for the Loess Plateau in northern China," *Agricultural Syst.*, vol. 79, no. 2, pp. 145–170, 2004.

[53] Y. He, Y. Zhang, and X. Yang, "Climate change in tropical area of southwestern China since 1950s," *Sci. Geogr. Sin.*, vol. 27, no. 4, 2007, Art. no. 499.

[54] H. Lü, D. Liu, and Z. Guo, "Natural vegetation of geological and historical periods in Loess Plateau," *Chin. Sci. Bull.*, vol. 48, no. 5, pp. 411–416, 2003.

[55] K. Zheng et al., "Impacts of climate change and human activities on grassland vegetation variation in the Chinese Loess Plateau," *Sci. Total Environ.*, vol. 660, pp. 236–244, 2019.

[56] C. J. Tucker et al., "An extended AVHRR 8-km NDVI dataset compatible with MODIS and SPOT vegetation NDVI data," *Int. J. Remote Sens.*, vol. 26, no. 20, pp. 4485–4498, 2005.

[57] R. De Jong, S. de Bruin, A. de Wit, M. E. Schaepman, and D. L. Dent, "Analysis of monotonic greening and browning trends from global NDVI time-series," *Remote Sens. Environ.*, vol. 115, no. 2, pp. 692–702, 2011.

[58] G. Bao, Z. Qin, Y. Bao, Y. Zhou, W. Li, and A. Sanjjav, "NDVI-based long-term vegetation dynamics and its response to climatic change in the Mongolian Plateau," *Remote Sens.*, vol. 6, no. 9, pp. 8337–8358, 2014.

[59] C. Eisfelder, C. Kuenzer, and S. Dech, "Derivation of biomass information for semi-arid areas using remote-sensing data," *Int. J. Remote Sens.*, vol. 33, no. 9, pp. 2937–2984, 2012.

[60] S. W. Running, R. R. Nemani, F. A. Heinsch, M. Zhao, M. Reeves, and H. Hashimoto, "A continuous satellite-derived measure of global terrestrial primary production," *Bioscience*, vol. 54, no. 6, pp. 547–560, 2004.

[61] S. Piao, J. Fang, W. Ji, Q. Guo, J. Ke, and S. Tao, "Variation in a satellite-based vegetation index in relation to climate in China," *J. Vegetation Sci.*, vol. 15, no. 2, pp. 219–226, 2004.

[62] B. N. Holben, "Characteristics of maximum-value composite images from temporal AVHRR data," *Int. J. Remote Sens.*, vol. 7, no. 11, pp. 1417–1434, 1986.

[63] B. Xie, X. Jia, Z. Qin, J. Shen, and Q. Chang, "Vegetation dynamics and climate change on the Loess Plateau, China: 1982–2011," *Regional Environ. Change*, vol. 16, no. 6, pp. 1583–1594, 2016.

[64] S. Piao, X. Wang, P. Ciais, B. Zhu, T. Wang, and J. Liu, "Changes in satellite-derived vegetation growth trend in temperate and boreal Eurasia from 1982 to 2006," *Glob. Change Biol.*, vol. 17, no. 10, pp. 3228–3239, 2011.

[65] Y. He, X. Guo, P. Dixon, and J. F. Wilmshurst, "NDVI variation and its relation to climate in Canadian ecozones," *Can. Geogr./ Géographe Can.*, vol. 56, no. 4, pp. 492–507, 2012.

[66] Z. Li and M. Kafatos, "Interannual variability of vegetation in the United States and its relation to El Nino/Southern Oscillation," *Remote Sens. Environ.*, vol. 71, no. 3, pp. 239–247, 2000.

[67] G. J. Jia, H. E. Epstein, and D. A. Walker, "Spatial heterogeneity of tundra vegetation response to recent temperature changes," *Glob. Change Biol.*, vol. 12, no. 1, pp. 42–55, 2006.

[68] Y. Bao, T. Xiong, and Z. Hu, "Forecasting air passenger traffic by support vector machines with ensemble empirical mode decomposition and slope-based method," *Discr. Dyn. Nature Soc.*, vol. 2012, 2012, Art. no. 431512.

[69] D. Wu et al., "Time-lag effects of global vegetation responses to climate change," *Glob. Change Biol.*, vol. 21, no. 9, pp. 3520–3531, 2015.

[70] Z. Wen, S. Wu, J. Chen, and M. Lü, "NDVI indicated long-term interannual changes in vegetation activities and their responses to climatic and anthropogenic factors in the Three Gorges Reservoir Region, China," *Sci. Total Environ.*, vol. 574, pp. 947–959, 2017.

[71] Y. Yin, D. Ma, S. Wu, E. Dai, Z. Zhu, and R. B. Myneni, "Nonlinear variations of forest leaf area index over China during 1982–2010 based on EEMD method," *Int. J. Biometeorol.*, vol. 61, no. 6, pp. 977–988, 2017.

[72] V. N. Vapnik, "An overview of statistical learning theory," *IEEE Trans. Neural Netw.*, vol. 10, no. 5, pp. 988–999, Sep. 1999.

[73] U. Thissen, R. van Brakel, A. P. de Weijer, W. J. Melssen, and L. M. C. Buydens, "Using support vector machines for time series prediction," *Chemometrics Intell. Lab. Syst.*, vol. 69, no. 1/2, pp. 35–49, 2003.

[74] N. I. Sapankevych and R. Sankar, "Time series prediction using support vector machines: A survey," *IEEE Comput. Intell. Mag.*, vol. 4, no. 2, pp. 24–38, May 2009.

[75] D. C. R. Novitasari, H. Rohayani, R. Junaidi, R. D. Setyowati, R. Pramulya, and F. Setiawan, "Weather parameters forecasting as variables for rainfall prediction using adaptive neuro fuzzy inference system (ANFIS) and support vector regression (SVR)," *J. Phys., Conf. Ser.*, vol. 1501, no. 1, 2020, Art. no. 012012.

[76] P. J. Luukko, J. Helske, and E. Räsänen, "Introducing libeemd: A program package for performing the ensemble empirical mode decomposition," *Comput. Statist.*, vol. 31, no. 2, pp. 545–557, 2016.

[77] L. Wang and Y. Shao, "Fault feature extraction of rotating machinery using a reweighted complete ensemble empirical mode decomposition with adaptive noise and demodulation analysis," *Mech. Syst. Signal Process.*, vol. 138, 2020, Art. no. 106545.

[78] H. Liu, M. Zhang, Z. Lin, and X. Xu, "Spatial heterogeneity of the relationship between vegetation dynamics and climate change and their driving forces at multiple time scales in Southwest China," *Agricultural Forest Meteorol.*, vol. 256, pp. 10–21, 2018.

[79] W. Sun, X. Song, X. Mu, P. Gao, F. Wang, and G. Zhao, "Spatiotemporal vegetation cover variations associated with climate change and ecological restoration in the Loess Plateau," *Agricultural Forest Meteorol.*, vol. 209, pp. 87–99, 2015.

[80] A. Zhao, A. Zhang, X. Liu, and S. Cao, "Spatiotemporal changes of normalized difference vegetation index (NDVI) and response to climate extremes and ecological restoration in the Loess Plateau, China," *Theor. Appl. Climatol.*, vol. 132, no. 1, pp. 555–567, 2018.

[81] C. J. Tucker, D. A. Slayback, J. E. Pinzon, S. O. Los, R. B. Myneni, and M. G. Taylor, "Higher northern latitude normalized difference vegetation index and growing season trends from 1982 to 1999," *Int. J. Biometeorol.*, vol. 45, no. 4, pp. 184–190, 2001.

[82] R. B. Myneni, C. D. Keeling, C. J. Tucker, G. Asrar, and R. R. Nemani, "Increased plant growth in the northern high latitudes from 1981 to 1991," *Nature*, vol. 386, no. 6626, pp. 698–702, 1997.

[83] L. Zhou, C. J. Tucker, R. K. Kaufmann, D. Slayback, N. V. Shabanov, and R. B. Myneni, "Variations in northern vegetation activity inferred from satellite data of vegetation index during 1981 to 1999," *J. Geophys. Res. Atmos.*, vol. 106, no. D17, pp. 20069–20083, 2001.

[84] S. Cao et al., "Effects and contributions of meteorological drought on agricultural drought under different climatic zones and vegetation types in Northwest China," *Sci. Total Environ.*, vol. 821, 2022, Art. no. 153270.

[85] S. M. Vicente-Serrano et al., "Response of vegetation to drought time-scales across global land biomes," *Proc. Nat. Acad. Sci. USA,* vol. 110, no. 1, pp. 52–57, 2013.

[86] X. W. Chuai, X. J. Huang, W. J. Wang, and G. Bao, "NDVI, temperature and precipitation changes and their relationships with different vegetation types during 1998–2007 in Inner Mongolia, China," *Int. J. Climatol.*, vol. 33, no. 7, pp. 1696–1706, 2013.

[87] S. D. Puntsukova, B. O. Gomboev, M. R. Akhmetzyanova, T. Jamsran, T. Dagdan, and D. Suocheng, "Comparative analysis of different forest ecosystems response to global climate change and economic activity," *J. Resour. Ecol.*, vol. 6, no. 2, pp. 106–109, 2015.

[88] S. Huang and J. Kong, "Assessing land degradation dynamics and distinguishing human-induced changes from climate factors in the Three-North Shelter Forest region of China," *ISPRS Int. J. Geo-Inf.*, vol. 5, no. 9, 2016, Art. no. 158.

[89] S. Liang, Q. Yi, and J. Liu, "Vegetation dynamics and responses to recent climate change in Xinjiang using leaf area index as an indicator," *Ecol. Indicators*, vol. 58, pp. 64–76, 2015.

[90] P. Molnar, W. R. Boos, and D. S. Battisti, "Orographic controls on climate and paleoclimate of Asia: Thermal and mechanical roles for the Tibetan Plateau," *Annu. Rev. Earth Planet. Sci.*, vol. 38, no. 1, pp. 77–102, 2010.
[91] Y. L. Hang, G. Bao, Y. H. Bao, and D. A. Burenjirigala, "Spatiotemporal changes of vegetation coverage in Xilin Gol Grassland and its responses to climate change during 2000–2010," *Acta Agrestia Sin.*, vol. 22, no. 6, 2014, Art. no. 1194.
[92] Q. Y. Zhang, S. H. Wu, D. S. Zhao, and E. F. Dai, "Responses of growing season vegetation changes to climatic factors in Inner Mongolia grassland," *J. Natural Resour.*, vol. 28, pp. 754–764, 2013.
[93] L. Zhang, X. Chen, X. Cai, and H. A. Salim, "Spatial-temporal changes of NDVI and their relations with precipitation and temperature in Yangtze River basin from 1981 to 2001," *Geo-Spat. Inf. Sci.*, vol. 13, no. 3, pp. 186–190, 2010.
[94] W. Hua et al., "Observational quantification of climatic and human influences on vegetation greening in China," *Remote Sens.*, vol. 9, no. 5, 2017, Art. no. 425.
[95] K. Ichii, A. Kawabata, and Y. Yamaguchi, "Global correlation analysis for NDVI and climatic variables and NDVI trends: 1982-1990," *Int. J. Remote Sens.*, vol. 23, no. 18, pp. 3873–3878, 2002.
[96] C. O. Justice, B. N. Holben, and M. D. Gwynne, "Monitoring East African vegetation using AVHRR data," *Int. J. Remote Sens.*, vol. 7, no. 11, pp. 1453–1474, 1986.
[97] H. Wei, X. Zhao, S. Liang, T. Zhou, D. Wu, and B. Tang, "Effects of warming hiatuses on vegetation growth in the Northern Hemisphere," *Remote Sens.*, vol. 10, no. 5, 2018, Art. no. 683.
[98] J.-T. Zhang, W. Ru, and B. Li, "Relationships between vegetation and climate on the Loess Plateau in China," *Folia Geobotanica,* vol. 41, no. 2, pp. 151–163, 2006.
[99] Y. Zhang et al., "Vegetation dynamics and its driving forces from climate change and human activities in the Three-River Source Region, China from 1982 to 2012," *Sci. Total Environ.*, vol. 563, pp. 210–220, 2016.

Qianqian Sun received the M.S. degree in geomatics engineering from the Anhui University of Science and Technology, Huainan, China, in 2021. She is currently working toward the Ph.D. degree in geomatics science and technology with the Faculty of Geosciences and Environmental Engineering, Southwest Jiaotong University, Chengdu, China.

Her research interests include remote sensing, 3-D visualization, and algorithmic analysis.

Tianyang Chen received the B.S. degree in survey engineering from the Hebei University of Engineering, Handan, China, in 2014, and the M.S. degree in geographic information science and cartography from the University of Eastern Michigan, Ypsilanti, MI, USA, in 2018. He is currently working toward the Ph.D. degree in geography with the University of North Carolina at Charlotte, Charlotte, NC, USA.

His research interests include spatial analysis, Web geographic information system (GIS), and deep learning-based 3-D point cloud classification.

Chao Liu received the Ph.D. degree in geodesy and surveying engineering from the China University of Mining and Technology, Xuzhou, China, in 2011.

He is currently an Associate Professor with the School of Spatial Information and Geomatics Engineering, Anhui University of Science and Technology, Huainan, China. His current research interests include global navigation satellite system (GNSS) signal processing, deep learning, and remote sensing.

Anbing Zhang received the Ph.D. degree in geodesy and surveying engineering from the China University of Mining and Technology, Xuzhou, China, in 2009.

He is currently an Associate Professor with the School of Mining and Geomatics, Hebei University of Engineering, Handan, China. His research interests include GPS data processing, deformation monitoring, and remote sensing applications.

Chunyang Liu received the Ph.D. degree in geodesy and surveying engineering from the China University of Mining and Technology, Xuzhou, China, in 2020.

He is currently a Lecturer with the School of Spatial Information and Geomatics Engineering, Anhui University of Science and Technology, Huainan, China. His current research interests include spatiotemporal big data analysis and deep learning.

Yuan Tao received the M.S. degree in geodesy and surveying engineering from the Anhui University of Science and Technology, Huainan, China, in 2021. He is currently working toward the Ph.D. degree in cartography and geographical information engineering with the School of Environment and Spatial Informatics, China University of Mining and Technology, Xuzhou, China.

His research interests include remote sensing, land cover classification, and change detection.